RESEARCH ARTICLE

# Ensemble forecasting of Indian Ocean Dipole events generated by conditional nonlinear optimal perturbation method

Rong Feng[1] | Wansuo Duan[1,2] | Lei Hu[1] | Ting Liu[3,4]

[1]LASG, Institute of Atmospheric Physics, Chinese Academy of Sciences, Beijing, China

[2]Collaborative Innovation Center on Forecast and Evaluation of Meteorological Disasters (CIC-FEMD), Nanjing University of Information Science and Technology, Nanjing, China

[3]State Key Laboratory of Satellite Ocean Environment Dynamics, Second Institute of Oceanography, Ministry of Natural Resources, Hangzhou, China

[4]Southern Marine Science and Engineering Guangdong Laboratory (Zhuhai), Zhuhai, China

**Correspondence**

Wansuo Duan, LASG, Institute of Atmospheric Physics, Chinese Academy of Sciences, Beijing 100029, China.
Email: duanws@lasg.iap.ac.cn

**Abstract**

In this study, we applied the conditional nonlinear optimal perturbation (CNOP) method to generate nonlinear fast-growing initial perturbations for ensemble forecasting, aiming to assess the effectiveness of the CNOP method in improving the forecast skill of climate events. Our findings reveal a significant improvement in the forecast skill of the Indian Ocean Dipole (IOD) within the CNOP ensemble forecast, particularly at long lead times, thereby extending the skilful forecast lead times. Notably, this improvement is more prominent for strong IOD events, with skilful forecast lead times exceeding 12 months, outperforming many current state-of-the-art coupled models. The high forecast skill of the CNOP method is primarily attributed to its ability to capture the uncertainties in the wind anomaly field in the eastern Indian Ocean (EIO) closely associated with IOD evolution. Consequently, CNOP ensemble members exhibit significant deviations from the control forecast, resulting in a large ensemble spread encompassing IOD evolution. Furthermore, a comparison with the climate-relevant singular vectors (CSV) method in terms of IOD and El Niño–Southern Oscillation (ENSO) predictions reveals the superior performance of the CNOP ensemble forecast. Despite the initial perturbations for ensemble forecasting being generated aimed at improving IOD forecast skill, the CNOP method significantly improves the forecast skill of both IOD and ENSO events, with a greater improvement for ENSO. Additionally, the CNOP ensemble forecast system provides more reliable estimates of forecast uncertainties and exhibits higher reliability with increasing lead times. In conclusion, the CNOP method effectively captures the nonlinear physical processes of climate events and improve the forecast skill.

**KEYWORDS**

ensemble forecasting, Indian Ocean Dipole, initial perturbations, nonlinearity

## 1 | INTRODUCTION

The Indian Ocean Dipole (IOD) is an important ocean–atmosphere coupled phenomenon of interannual timescale in the tropical Indian Ocean, which exhibits a west–east seesaw pattern of sea surface temperature anomalies (SSTAs) along with anomalous wind field at the equator (Saji et al., 1999; Webster et al., 1999). Not

only do IOD events cause severe natural disasters in coastal regions (Ansell et al., 2000), they also influence weather and climate in distant areas through planetary atmospheric waves (Saji & Yamagata, 2003). With greenhouse warming, the frequency of extreme IOD events is on the rise (Cai et al., 2020; Huang et al., 2019; Hui & Zheng, 2018). Previous studies have revealed that most numerical models can skilfully predict IOD events only up to one season in advance, extending to two seasons for strong events (Luo et al., 2005, 2007; Shi et al., 2012; Zhao & Hendon, 2009).

Ensemble forecasting is one important method for reducing prediction uncertainties in weather and climate events and improving forecast skill. The traditional ensemble forecasting is an initial value problem, and the ensemble forecast skill relies on the quality of initial perturbations (Du et al., 2019). Ensemble generation methods can be generally distinguished used in numerical weather predcition (NWP) and climate/seasonal predictions. The sophisticated methods like singular vectors (SVs; Leutbecher & Palmer, 2008; Lorenz, 1965) and bred vectors (BVs; Toth & Kalnay, 1993), separately used by the European Centre for Medium-Range Weather Forecasts (ECMWF) and the National Centers for Environmental Prediction (NCEP), are mostly adopted for NWP. SVs method has clear dynamic significance, but adopts linear approximation to numerical models, so the initial perturbations generated by the SVs method cannot well reflect the role of nonlinear physical processes in the weather and climate systems (Anderson, 1997). BVs are obtained from long-term model integrations before the start of the prediction, which may not exhibit rapid growth dynamics during the prediction period (Du et al., 2019; Zhang et al., 2023). Furthermore, Ensemble Kalman filter (ENKF; Evensen, 1994) and Ensemble Transform Kalman filter (ETKF; Houtekamer & Derome, 1994) assimilation methods are also employed in NWP, but like BVs, they describe initial perturbations obtained before the prediction start time, and cannot guarantee the rapid growth dynamics needed during the prediction period. In order to overcome the linear limitation of SVs method, Duan and Huo (2016) has developed the orthogonal conditional nonlinear optimal perturbation (O-CNOP) ensemble forecast method, which not only considers the effects of nonlinear physical processes, but also characterizes the fast-growing initial perturbations during the prediction period. The O-CNOP method has been utilized in the ensemble forecast of weather events (Duan & Huo, 2016; Huo & Duan, 2018; Zhang et al., 2023). Using typhoons as an example, the O-CNOP method has shown remarkable performance in typhoon track ensemble forecasting, effectively reducing prediction errors and exhibiting higher forecast skill in

predicting landing sites, landing times and track turning compared to SVs and BVs (Duan et al., 2023; Huo & Duan, 2018; Zhang et al., 2023).

So far, the methods mentioned above are mostly adopted in NWP. Their applications in climate predictions are limited or only partially applied in the atmospheric component of a coupled system. For example, in the ECMWF, SVs method was applied for its atmospheric initial conditions, while perturbed ocean states are generated by random perturbations in its ocean data assimilation analysis. Recognizing the crucial importance of adequately sampling uncertainty in oceanic initial conditions in climate predictions, numerous methods that take into account structural uncertainty in oceanic initial conditions have been developed and implemented in climate predictions (Duan et al., 2024; Kleeman et al., 2003; Liu et al., 2022; Zhu et al., 2013, 2015). In the NCEP, the Climate Forecast System version 2 (CFSv2) applies the lagged ensemble (LE) approach which generates ensemble members with initial conditions at different times (Zhu et al., 2015). The LE method has the potential of sampling the different phases of high-frequency phenomena such as Madden–Julian oscillation (MJO) or Tropical Instability Wave (TIW) which may have strong effect on evolutions of climate modes (e.g., El Niño–Southern Oscillation [ENSO], IOD) and thus their predictions. Kleeman et al. (2003) introduced the climate-relevant SV (CSV) method, which employs the ensemble method to compute the SVs. Through the ensemble-mean method, the weather-scale noise can be filtered out to retain the fast growing mode of the climate scale. Liu et al. (2022) applied this method in conducting ENSO ensemble forecast, significantly improving ENSO forecast skill. To expand the application of O-CNOP to climate predictions, a novel approach called coupled CNOP (C-CNOP) has been developed (Duan et al., 2024). While retaining the advantage of the O-CNOP method in considering nonlinear unstable-growing initial perturbations, the C-CNOP method can also depict initial coupling uncertainties across different components of the earth system. The C-CNOP method has been utilized in ENSO ensemble forecasting, successfully capturing initial ocean–atmosphere coupling uncertainties, even weak initial coupling information for predictions initiated in the spring and summer, thereby weakening the spring predictability barrier (SPB) and improving ENSO forecast skill.

Although previous studies have utilized ensemble forecasting strategies to discuss IOD predictions, the methods adopted have significant limitations in terms of dynamic significance and characterization of nonlinear effects, resulting in low prediction skills for the IOD (Du et al., 2020; Luo et al., 2007; Shi et al., 2012; Zhu

et al., 2015). For instance, Zhu et al. (2015) utilized model analysis fields at different times before the initial forecast time to generate ensemble forecast members, with successful prediction of IOD events less than one season in advance. Stockdale et al. (2011) generated ensemble members using the SVs method in the ECMWF seasonal forecast system. However, due to the linear approximation of the SVs, the ensemble forecast system could not effectively extend the lead time of skilful forecasting for IOD events. Shi et al. (2012) further assessed the prediction skills of four prediction systems that generated ensemble members using the EnKF, SVs and other methods, showing that these four ensemble forecast systems could only forecast IOD events about one season in advance. Given these limitations, the C-CNOP method will be employed in this study to improve the skill of IOD ensemble forecasting. A comparison with the CSV method is also conducted to further explore the advantage of the C-CNOP method. Since the CSV method is unable to describe initial coupling uncertainties, the C-CNOP method will solely focus on ocean temperature perturbations, which is referred as the CNOP method in subsequent discussions. Several questions are addressed in this paper: if the CNOP method is applied in IOD ensemble forecasting, will it improve the IOD forecast skill and extend the lead time of skilful forecast? Additionally, what are the advantages of the CNOP method compared with the CSV method?

To address these issues, the paper is structured as follows. Section 2 introduces the CNOP method and the model. Section 3 examines the application of the CNOP method in IOD ensemble forecasting. The prediction results of the CNOP and CSV methods are compared in section 4. Finally, a summary and discussion are presented in section 5.

## 2 | MODEL, DATA AND METHOD

### 2.1 | Model and data

The Geophysical Fluid Dynamics Laboratory Climate Model version 2p1 (GFDL CM2p1), an ocean-atmosphere-ice-land coupled model, is utilized in this study. The oceanic component is the Modular Ocean Model version 4 (MOM4p1; Griffies, 2009), with a horizontal resolution of $1 \times 1$ in most regions and a meridional resolution reduced to 1/3 at the equator. There are a total of 50 vertical levels with a 10-m resolution in the upper 225 m. The atmospheric model is the GFDL atmosphere model, AM2p12b (GFDL Global Atmospheric Model Development Team, 2004), with a horizontal resolution

of $2.5 \times 2$ and a total of 24 vertical levels. The different model components are coupled and exchange fluxes through the Flexible Modeling System. Previous studies have demonstrated that the GFDL CM2p1 coupled model effectively simulates the Indian Ocean climatology and reproduces the basic characteristics of IOD events (Feng et al., 2014; Song et al., 2008). Therefore, it is reasonable to utilize this model for the study of IOD ensemble forecast.

The ocean temperature data from the Simple Ocean Data Assimilation (SODA 2.2.4; Carton & Giese, 2008) was assimilated into the oceanic initial field in the GFDL CM2p1 using the nudging data assimilation algorithm. The assimilation area covers the global ocean horizontally and extends to 500 m in the upper ocean vertically. The assimilation period spans from 1969 to 2008. The initial field, with oceanic observations assimilated, exhibits high correlation coefficients with observational datasets, particularly in the upper tropical Pacific Ocean (figure omitted). This indicates that the nudging algorithm effectively assimilated oceanic temperature observations into the model and produced an accurate initial field. The initial field is further used to run the GFDL CM2p1 from 1979 to 2008 and generate the control forecast (referred to as the CTRL).

### 2.2 | The CNOP method

Feng et al. (2017) illustrated that the spatial patterns of fast-growing initial errors are independent of IOD events, but vary with the start months of IOD predictions. Consequently, the phase-space bases of the fast growing initial perturbations for ensemble forecast are derived from these fast-growing initial errors at different start months, which characterize the primary modes of initial perturbations that exert a substantial influence on IOD predictions. According to the amplitude characteristics of the initial analysis errors in the CTRL, these bases are further expanded into a nonlinear phase space that captures the rapidly growing initial perturbations at the forecast start month through vector linear combinations. Subsequently, an IOD ensemble forecast is conducted using the initial perturbation samples within this space. In this study, the initial errors that result in the largest prediction uncertainties in IOD events were initially identified. By obtaining fast-growing initial errors of various IOD events, we established the basis of phase space of these rapidly growing perturbations and then generated initial perturbation samples for IOD ensemble forecast. A brief introduction to the method is as follows, and for more details, please refer to Duan et al. (2024).

The variation of state vector $Q$ can be written as

$$\begin{cases} \dfrac{dQ}{dt} = F(Q,t) + f \\ Q|_{t=0} = Q_0 \end{cases}, \text{ in } \Omega \times [0, T], \qquad (1)$$

where $F$ is a nonlinear operator, $t$ is time, $t \in [0, T]$, $T < +\infty$, $Q_0$ denotes the initial state of $Q$, $f$ is the external forcing, which is constant in the GFDL CM2p1 integration. Equation (1) can be rewritten as follows:

$$dQ = F(Q,t)dt + fdt. \qquad (2)$$

Equation (2) is then integrated from times $t_a$ to $t_b$ ($t_a < t_b < T$) and gets Equation (3),

$$\int_{t_a}^{t_b} dQ = \int_{t_a}^{t_b} F(Q,t)dt + \int_{t_a}^{t_b} fdt = \int_{t_a}^{t_b} F(Q,t)dt + f(t_b - t_a). \qquad (3)$$

Therefore, the predicted variable $Q_{t_b}$ in the future time $t_b$ can be stated as follows:

$$Q_{t_b} = Q_{t_a} + \int_{t_a}^{t_b} F(Q,t)dt + f(t_b - t_a). \qquad (4)$$

According to Equation (4), if two time periods $[t_{01}, t_1]$ and $[t_{02}, t_2]$ have the same length and are adopted from the model output datasets, then their respective initial states are $Q_{t_{01}}$ and $Q_{t_{02}}$, and their final states $Q_{t_1}$ and $Q_{t_2}$ can be stated as follows:

$$Q_{t_1} = \int_{t_{01}}^{t_1} Fdt + Q_{t_{01}} + f(t_1 - t_{01}), \qquad (5)$$

$$Q_{t_2} = \int_{t_{02}}^{t_2} Fdt + Q_{t_{02}} + f(t_2 - t_{02}). \qquad (6)$$

As the two time periods have the same length, Equation (6) minus Equation (5) gets Equation (7),

$$Q_{t_2} - Q_{t_1} = Q_{t_{02}} - Q_{t_{01}} + \left( \int_{t_{02}}^{t_2} Fdt - \int_{t_{01}}^{t_1} Fdt \right). \qquad (7)$$

Equation (7) can be rewritten as the same form as Equations (5) and (6),

$$Q_{t_2} - Q_{t_1} = Q_{t_{02}} - Q_{t_{01}} + \int_{\Sigma} [F_{t_{02}} - F_{t_{01}}]dt, \qquad (8)$$

where $F_{t_{02}}$ ($F_{t_{01}}$) represents the $F$ in Equation (6) (Equation (5)), and the $\Sigma$ is the time period $[t_{02}, t_2]([t_{01}, t_1])$. Obviously, the difference between the $Q_{t_1}$ and $Q_{t_2}$ is caused by the initial difference between $Q_{t_{01}}$ and $Q_{t_{02}}$. If the data series during the time period $[t_{01}, t_1]$ is seen as the "observation," and the data series corresponding to the time period $[t_{02}, t_2]$ can be seen as the "prediction" of the "observation." The prediction errors are only caused by the initial difference between $Q_{t_{02}}$ and $Q_{t_{01}}$.

The GFDL CM2p1 was run for 150 years with external forcings of land cover, insolation, aerosols and tracer gases in 1990. The last 100 years of output data were analysed to exclude the impact of initial adjustment process during the first 50-year spin up. All 11 positive IOD events were selected as "observations" from this 100-year dataset. For each of the one-year "observation," the other 99 1-year data can be seen as the "predictions" corresponding to this "observation." Consequently, for every "observation," there were totally 99 "predictions." The prediction errors were calculated as the absolute difference in the Dipole Mode Index (DMI) values between each "observation" and its corresponding "prediction," which are only caused by the initial errors as stated above. The DMI here represents the SSTA difference between the western Indian Ocean (WIO; 50°–70°E, 10°S–10°N) and the eastern Indian Ocean (EIO; 90°–110°E, 10°S–0°) as defined in Saji et al. (1999). The growth rates of these prediction errors $G$ are expressed as follows:

$$G = \frac{\partial P_t}{\partial t} \approx \frac{P_{t_2} - P_{t_1}}{t_2 - t_1}, \qquad (9)$$

where $P_{t_2}$ and $P_{t_1}$ denote the prediction errors at times $t_2$ and $t_1$, with a 1-month interval between them. The positive $G$ signifies an increase in prediction errors, with higher values indicating faster increase of prediction errors; and vice versa for negative $G$. By summing the $G$ values over a season, the seasonal growth rates of prediction errors can be derived. Consequently, initial errors yielding the largest positive $G$ values during boreal winter or summer, which induce a significant winter or summer predictability barrier, are chosen and deemed to have the most significant influence on IOD predictability. There are a large amount of "prediction" series which guarantee the diversity and statistical significance. That is, these initial errors are chosen based on finite but statistically significant "prediction" samples. As previously mentioned, CNOP denotes the initial errors that yield the largest prediction uncertainties at the prediction time under specific constraint condition (Mu et al., 2003). Consequently, when the finite but statistically significant "prediction" samples are regarded as the constraint condition, the initial errors derived through this method are statistically

optimal and denoted as CNOP. CNOP here signifies initial errors that have the most pronounced effect on prediction uncertainty for IOD events within the GFDL CM2p1 model.

Following the steps above, we calculated the CNOP for forecasts starting from January, April, July and October, each with a 12-month lead time. For every starting month, a total of 11 CNOPs were derived corresponding to 11 "observations." Similarly, we identified initial errors that led to the 2nd to 5th highest growth rates in prediction errors during either the boreal winter or summer, considering them as the fast-growing initial errors. Consequently, there are totally 55 fast-growing initial errors for each start month, and collectively called the CNOPs. The phase-space bases of rapidly growing initial perturbations for ensemble forecasts are extracted from the modes of these fast growing initial errors at the corresponding forecast start month, and these bases can describe the key modes of the initial errors that significantly impact on IOD predictions for that specific prediction start month. Then we expand these bases into a nonlinear phase space that captures rapidly growing initial perturbations at the prediction start month through vector linear combinations. Subsequently, an IOD ensemble forecast is conducted using the initial perturbation samples within this space. Based on above ideas, we employ empirical orthogonal function (EOF) analysis on the global ocean temperature within the upper 200 m of the 55 CNOPs for every prediction start month to extract the leading 30 modes, denoted as $E_i$ ($i = 1, 2, 3, ..., 30$, with an explanatory variance exceeding 90%). By combining these leading 30 modes linearly, we derive initial perturbations, denoted by $IP = \alpha_1 E_1 + \alpha_2 E_2 + \cdots + \alpha_{30} E_{30}$, and $\alpha_i$ is constant. Through the application of varying constant coefficients, five initial perturbations (IPs) covering the upper 200 m of the global ocean are generated for each starting month between 1979 and 2008. These perturbations significantly influence the uncertainties in IOD predictions and serve as the fast growing initial perturbations for IOD ensemble forecast. The magnitude of these IPs is determined by the amplitude characteristics of the initial analysis errors in the CTRL at the corresponding prediction start month.

# 3 | UTILIZING THE CNOP METHOD IN IOD ENSEMBLE FORECAST

## 3.1 | The ensemble forecast skill of IOD events utilizing the CNOP method

By adding and subtracting 5 IPs to and from the initial field of the control forecast and subsequently running the GFDL CM2p1 model for 12 months, we generated 10 perturbed predictions for each starting month of prediction. These predictions, alongside the CTRL, results in a total of 11 ensemble members. The ensemble forecasting is conducted from January 1979 to December 2008, with forecast starting from January, April, July and October of each year.

Figure 1 illustrates the anomaly correlation coefficients (ACCs) and root-mean-square error (RMSE) values for different experiments as functions of the lead time for DMI, EIO and WIO. An ACC exceeding 0.5 typically signifies a skilful forecast (Luo et al., 2005). Initially, the ACC of the DMI in the persistence forecast presents high values within the first two lead months, then decreasing rapidly, and achieving skilful forecasts solely at a 2-month lead time. The ACC in the CTRL experiment is lower than that in the persistence forecast during the initial two lead months, but beats the persistence forecast in the subsequent months. This suggests that through assimilating observations into the GFDL CM2p1 model to obtain a relatively accurate initial field, the CTRL improves the forecast skill for IOD events. The ACC in the CNOP ensemble-mean forecast is notably higher than that in the CTRL, particularly at long lead times, marking a significant improvement in IOD forecast skill. The improvement, defined as the difference in forecast skill between the two experiments, becomes more evident with increasing lead times, ultimately extending the lead times of skilful forecast. This improvement probably results from the CNOP method's capability to capture the nonlinear physical processes during IOD development compared to the CTRL experiment. The CNOP ensemble-mean forecast skilfully predict IOD events with a lead time of 4 months, showing comparable, or even superior performance to previous studies (Luo et al., 2007; Shi et al., 2012). The enhanced skill of the CNOP ensemble forecast is also reflected in forecasting ocean temperature in the EIO and WIO. Specifically, the EIO (WIO) achieves skilful forecasts within the initial 5-month (8-month) lead times, exhibiting higher forecast skill compared to the CTRL, particularly at long lead times. To further explore the advantages of the CNOP method in IOD ensemble forecast, the ACC for strong IOD events (i.e., those where the amplitude of the observed DMI exceeds one standard deviation for at least 5 months) is also analysed. Remarkably, the ACC for strong IOD events was higher than that for all events in both the CTRL and CNOP ensemble-mean forecasts in terms of the DMI, EIO and WIO. A comparison between the CNOP ensemble-mean forecast and the CTRL experiment revealed an improvement in forecast skill for strong IOD events, with the improvement becoming more obvious with increasing lead months. Notably, this improvement was more significant for
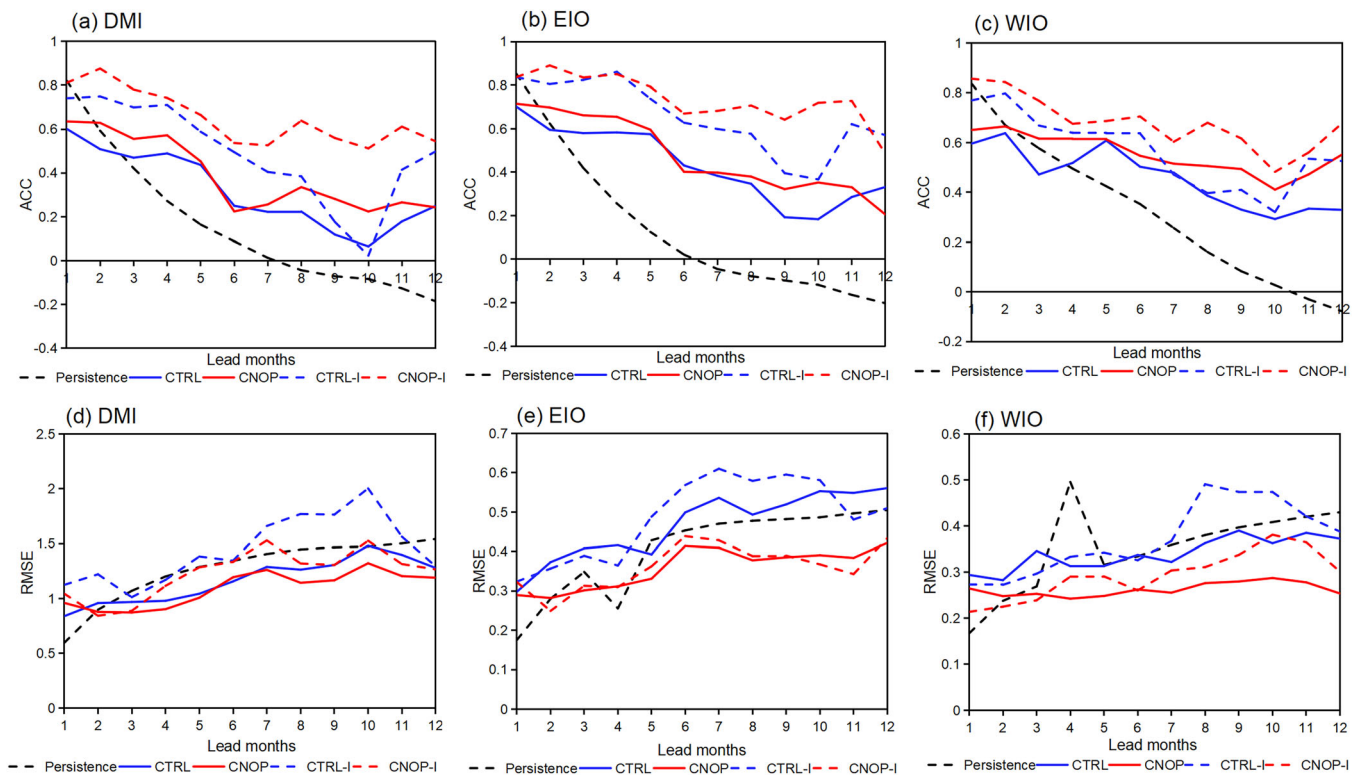
**FIGURE 1** Evolution of ACC for (a) DMI, (b) EIO and (c) WIO during 1979–2008 with respect to lead months; (d)–(f) denote corresponding RMSE values. Black dashed lines are for persistence forecast; blue and red solid lines are for all events in the CTRL and CNOP ensemble-mean forecasts, respectively; while blue and red dashed lines are for strong IOD events in the CTRL and CNOP ensemble-mean forecasts, respectively. [Colour figure can be viewed at wileyonlinelibrary.com]

strong IOD events compared to that for all events. These results confirm the CNOP method's ability to capture the nonlinear physical progresses associated with IOD events and improve forecast skill, particularly at long lead times. The lead time for a skilful forecast of strong IOD events exceeds 12 months in the CNOP ensemble-mean forecast, outperforming many current state-of-the-art coupled models (Luo et al., 2007; Shi et al., 2012). Most findings for RMSE are consistent with those for the ACC, with higher ACC values corresponding to lower RMSE values. However, the RMSE for strong IOD events was greater than that for all events in both the CTRL and CNOP ensemble-mean forecasts, indicating that strong IOD events may exhibit larger prediction errors compared to all events.

The time evolution of both predicted and observed DMI values at various lead times is represented in Figure 2. Notably, at lead times of 1 and 4 months, most IOD events are well predicted, with a more accurate amplitude in the CNOP ensemble-mean forecast compared to the CTRL. While the CTRL manages to capture some strong IOD events up to 7 months in advance, it fails to predict the strong IOD event in 1997 at a lead time of 10 months. In contrast, the positive IOD event in

1997 is successfully predicted with an accurate amplitude in the CNOP ensemble-mean forecast at a 10-month lead time. By comparing correlation skills of the DMI in the CNOP ensemble-mean forecast and the CTRL (reflected in the values in the top right corner of each graph), the CNOP ensemble-mean forecast has higher skill values and greatly improved the IOD forecast skill, particularly evident at longer lead times. This may be attributed to the CNOP method' ability to consider rapidly growing initial perturbations with nonlinear effects in the ensemble forecast.

In the following discussions, we will further analyse the horizontal distributions of the ACC at 1, 4, 7 and 10-month lead times in Figure 3. Although the initial perturbations in the CNOP ensemble forecast are primarily generated aimed at improving IOD forecast skill, the ACC in the tropical Pacific Ocean is also analysed. Our findings reveal that the ACC exceeding 0.5 is mainly concentrated in the southeastern Indian Ocean at a 4-month lead time in both the CTRL and CNOP ensemble-mean forecast. While the regions with the ACC exceeding 0.5 are located in the central Pacific Ocean at a 7-month lead time in the CTRL and at a 10-month lead time in the CNOP ensemble-mean forecast. This indicates that
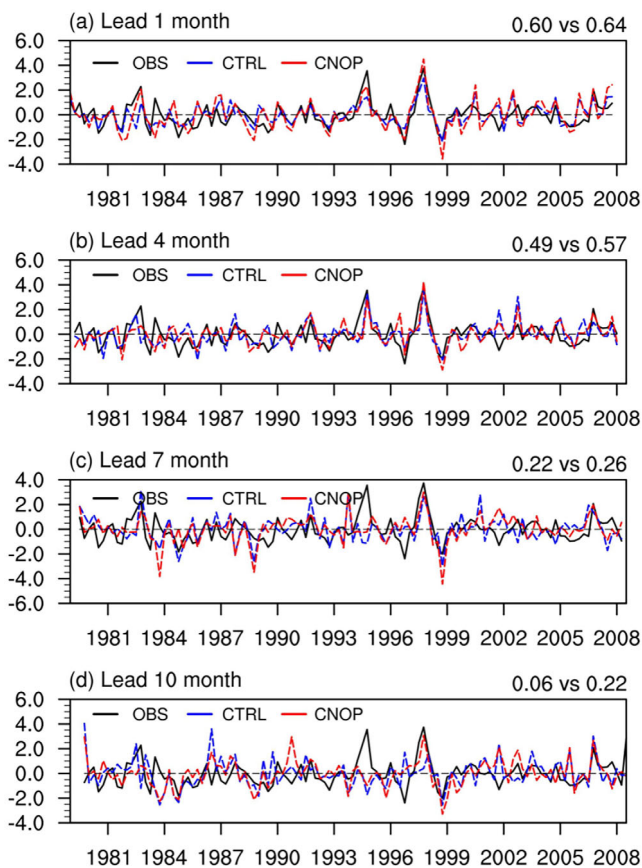
**FIGURE 2** Time series of the DMI in the observations, CTRL and CNOP ensemble-mean forecast at a 1, 4, 7 and 10-month lead time. The left (right) numbers in the top right corner describe the correlation skill between the time series of observations and the CTRL (the CNOP ensemble-mean forecast). [Colour figure can be viewed at wileyonlinelibrary.com]

the high forecast skill is mainly concentrated in the central Pacific Ocean even at a 10-month lead time in the CNOP ensemble forecast, which is significantly larger than that in the tropical Indian Ocean. The difference in ACC between the two prediction experiments is almost positive in both the tropical Indian and Pacific oceans, and becomes obvious with the increasing lead times. This indicates that the CNOP ensemble-mean forecast considerably improves the prediction skill across the tropical Indian and Pacific oceans with the improvement becoming particularly pronounced as the lead time increases. These findings support the view that the CNOP ensemble forecasting members could better capture the nonlinear physical processes of climate events in tropical oceans, leading to higher forecast skill, particularly at longer lead times. It is worth highlighting that although the CNOP initial perturbations are generated focused on IOD events, the ACC improvement in the tropical Pacific Ocean is almost positive, notably in the central and eastern Pacific Ocean, thereby significantly improving the ENSO forecast skill. As demonstrated in previous studies

(Shi et al., 2012; Wajsowicz, 2005), the WIO has a close relation with ENSO; therefore, the improvement of ENSO forecast skill, in turn, improves the forecast skill in the WIO.

Similarly, we also analysed the RMSE in the tropical oceans, as shown in Figure 4. The large values of RMSE are mainly concentrated in the EIO and the equatorial Pacific Ocean in the CTRL. That is, the prediction errors in these regions are large and challenging to be predicted. The RMSE difference between the CNOP ensemble-mean forecast and the CTRL presents negative values across most tropical oceans especially at longer lead times, with large absolute values concentrated in the EIO and the equatorial Pacific Ocean. This signifies a substantial reduction in prediction errors within these regions by conducting the CNOP ensemble forecasting, thereby greatly improving the forecast skill of IOD and ENSO events. Notably, this improvement becomes more obvious with increasing lead times.

In addition to examining the spatial distribution characteristics of forecast skill, a closer look at the seasonal variability of forecast skill in different experiments was conducted. As illustrated in Figure 5, the ACC skill of the DMI in both the CTRL and CNOP ensemble-mean forecasts as a function of lead time and start month was analysed. Notably, the forecast skills in both the CTRL and CNOP ensemble-mean forecasts show significant seasonal dependence. Predictions initiated in January and April displayed lower skill, whereas forecasts initiated in July and October presented higher skill. This seasonal variability highlights a notable winter predictability barrier (WPB) phenomenon, wherein forecast skill declines rapidly throughout the boreal winter irrespective of the start month (Feng et al., 2017; Luo et al., 2007). The CNOP ensemble-mean forecast skill decreases more rapidly throughout the boreal winter compared to the CTRL, suggesting a stronger WPB phenomenon. Additionally, the CNOP ensemble-mean forecast has a higher correlation skill than the CTRL and greatly improves forecast skills, particularly for predictions initiating in July and October.

## 3.2 | Why does the CNOP method provide higher ensemble forecast skill?

The above section has demonstrated that the CNOP ensemble-mean forecast exhibits higher skill compared to the CTRL experiment. In this section, we use the IOD event in 1997 as an example to delve into potential reasons for this high forecast skill. The IOD in 1997 is predicted from January in Figure 6. The results show that the CNOP ensemble-mean forecast successful predicts the strong IOD event peaking in October, whereas a normal event is observed in the CTRL experiment.
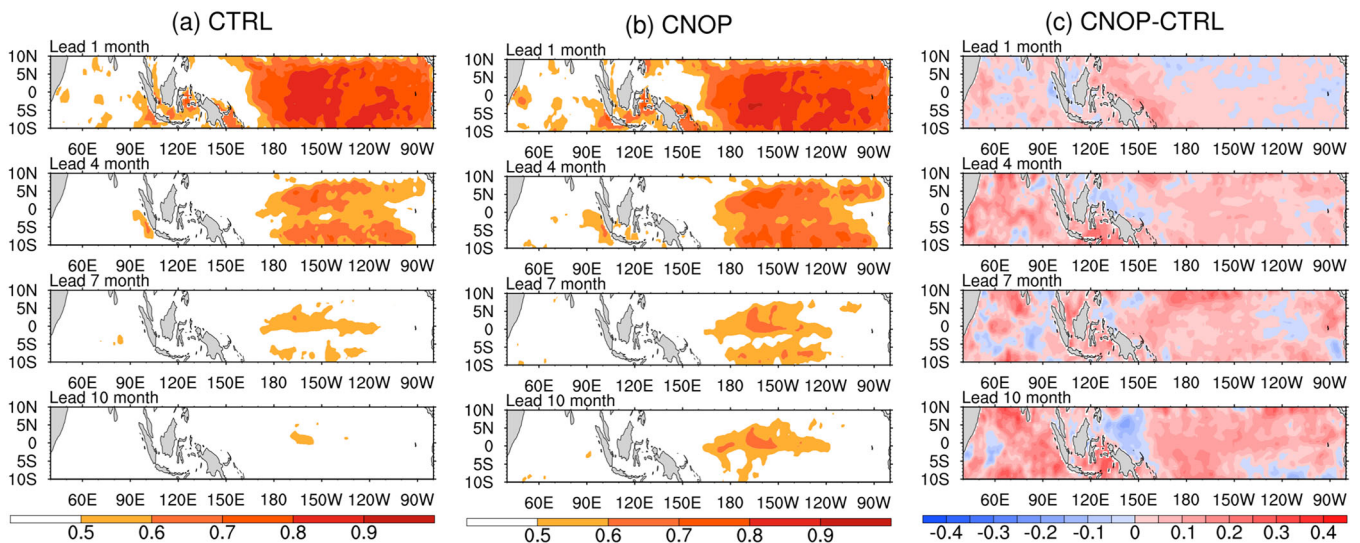
**FIGURE 3** Horizontal distributions of correlation skill for DMI in the (a) CTRL, (b) CNOP ensemble-mean forecast and (c) correlation skill difference between the CNOP ensemble-mean forecast and CTRL at a 1, 4, 7 and 10-month lead time, and the shaded areas in (a) and (b) are above 0.5. The results were obtained for all of the forecasts made during the period 1979–2008 regardless of their starting months. [Colour figure can be viewed at wileyonlinelibrary.com]
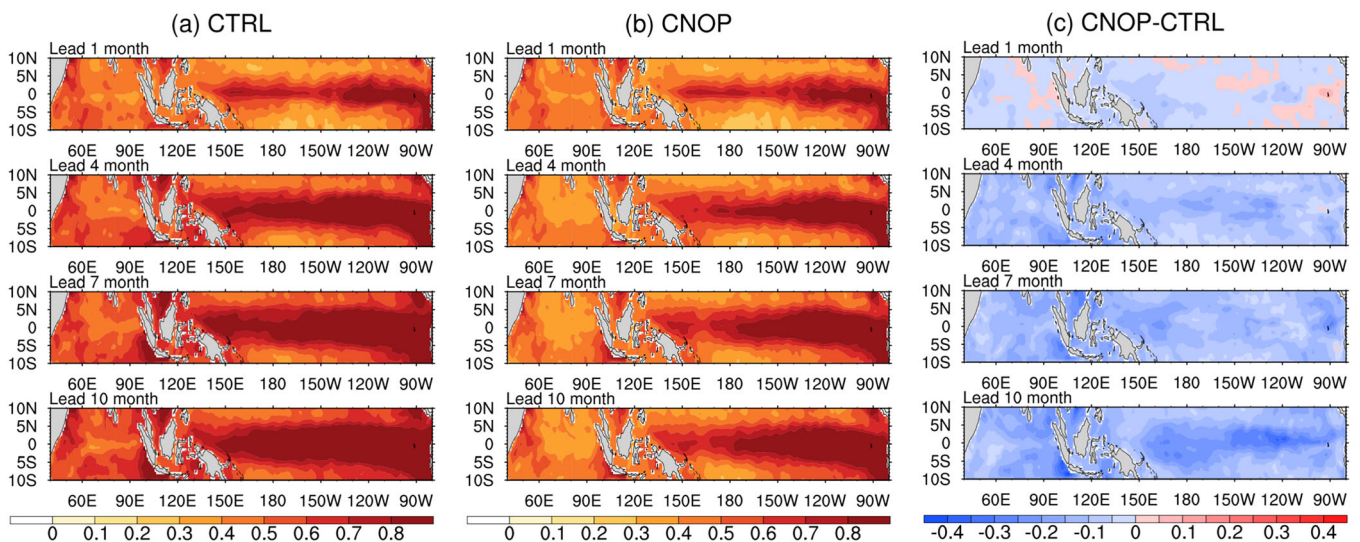


**FIGURE 4** The same as in Figure 3, but for the RMSE (units:°C). [Colour figure can be viewed at wileyonlinelibrary.com]

The analysis of the evolution of SSTAs and sea surface wind anomalies in the tropical Indian and Pacific oceans in 1997 is conducted in Figure 7. In March, southeasterly anomalies observed in the EIO in the observations promote offshore currents. This leads to the upwelling of the cold water, resulting in negative SSTAs in the EIO. Then under the Bjerknes feedback, a west–east dipole mode appears in the tropical Indian Ocean and a positive IOD event occurs. The crucial role of southeasterly anomalies in the EIO in the development of IOD events has also been highlighted in previous studies (Saji et al., 1999; Webster et al., 1999). However, the CTRL experiment fails to capture this key signal and instead shows

southwest wind anomalies in the EIO in March, causing water piling up and leading to positive SSTAs. In contrast, the CNOP ensemble-mean forecast successfully captures the southeasterly wind anomalies in the EIO and predicts the positive IOD event in 1997. This underscores the sensitivity of IOD forecasts to uncertainties in wind anomalies in the EIO. The zonal and meridional wind components in the tropical Indian Ocean in the CNOP ensemble forecast exhibit a large spread in the EIO at different lead months, as shown in Figure 8, capturing the uncertainty in wind anomalies in the EIO. That is, the CNOP ensemble forecast effectively describes the uncertainties in key processes influencing IOD
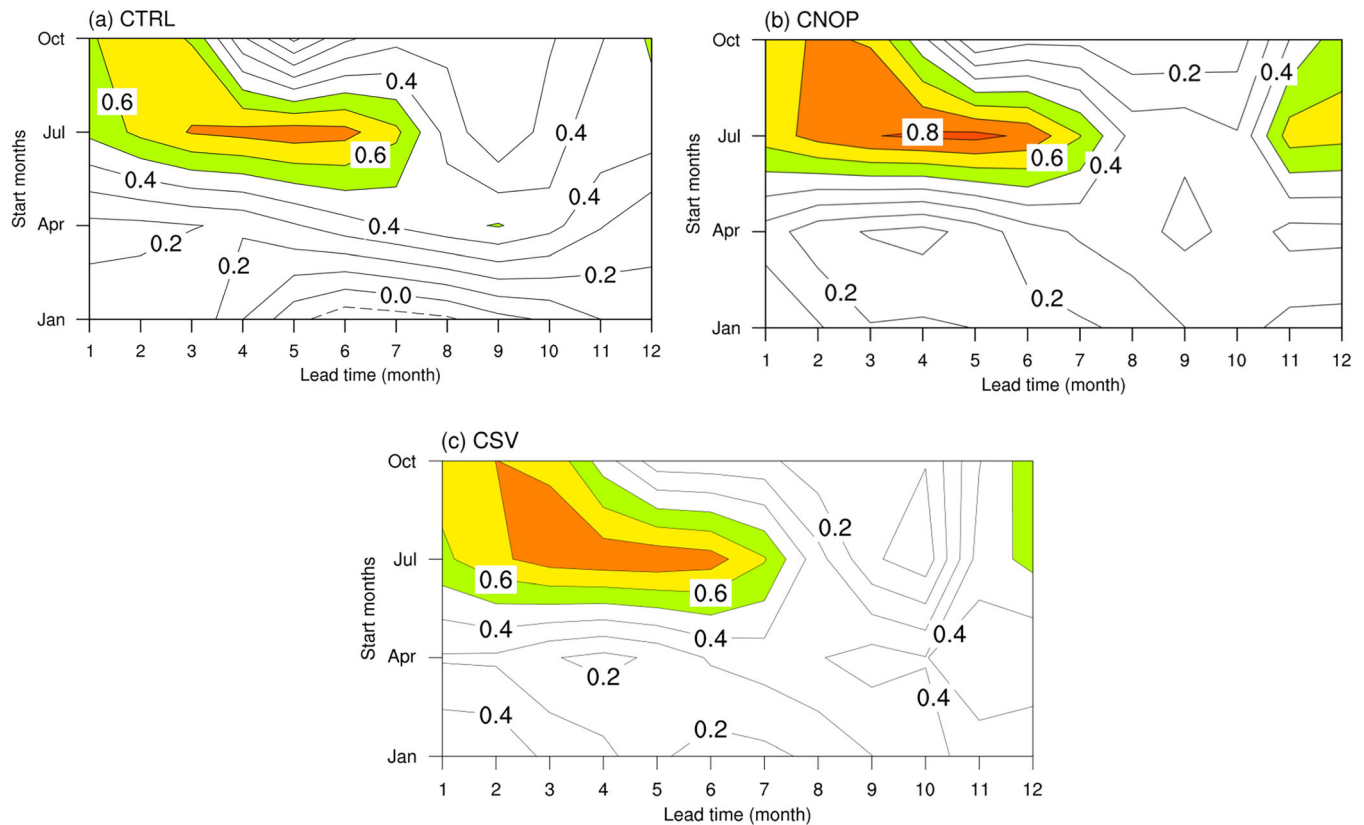
**FIGURE 5** ACC skill of the DMI as a function of the lead time and start month initiated on 1 January, 1 April, 1 July and 1 October in the (a) CTRL, (b) CNOP ensemble forecast and (c) CSV ensemble forecast. The coloured areas denoted ACC above 0.5. [Colour figure can be viewed at wileyonlinelibrary.com]
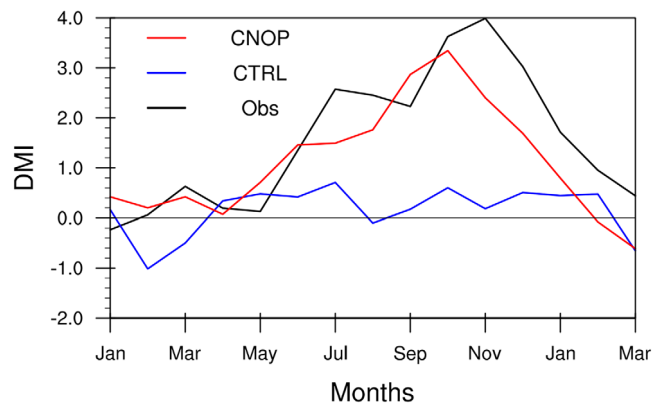


**FIGURE 6** Time series of the DMI in 1997 predicted from January in the observation, CTRL and CNOP ensemble-mean forecast. [Colour figure can be viewed at wileyonlinelibrary.com]

development, yielding ensemble members that diverge substantially from the control forecast and provide a large ensemble spread encompassing IOD development. This may explain the higher skill caused by the CNOP ensemble forecast for IOD events.

Moreover, although the southeasterly anomalies eventually appear in the EIO in May in the CTRL experiment, promoting the upwelling of cold water and the subsequent emergence of negative SSTAs in the EIO in July, the tropical Indian Ocean exhibits basin-wide negative SST anomalies in September instead of the expected west–east dipole pattern. This deviation is primarily attributed to the cooling influence of longwave and latent heat flux anomalies in the western Indian Ocean (figure omitted). Therefore, the absence of the anticipated positive IOD event in 1997 in the CTRL experiment can be largely attributed to the inaccurate forecast of both the wind anomaly field and the heat flux anomalies in the tropical Indian Ocean. It can be inferred that accurate predictions of these crucial factors are essential for improving the forecast skill of IOD events.

## 4 | COMPARISON OF ENSEMBLE FORECAST SKILLS WITH THE CSV METHOD

### 4.1 | Forecast skill of IOD and ENSO events

In the introduction, the CSV method, developed by Kleeman et al. (2003), is introduced for computing singular vectors in the absence of the adjoint model. In this
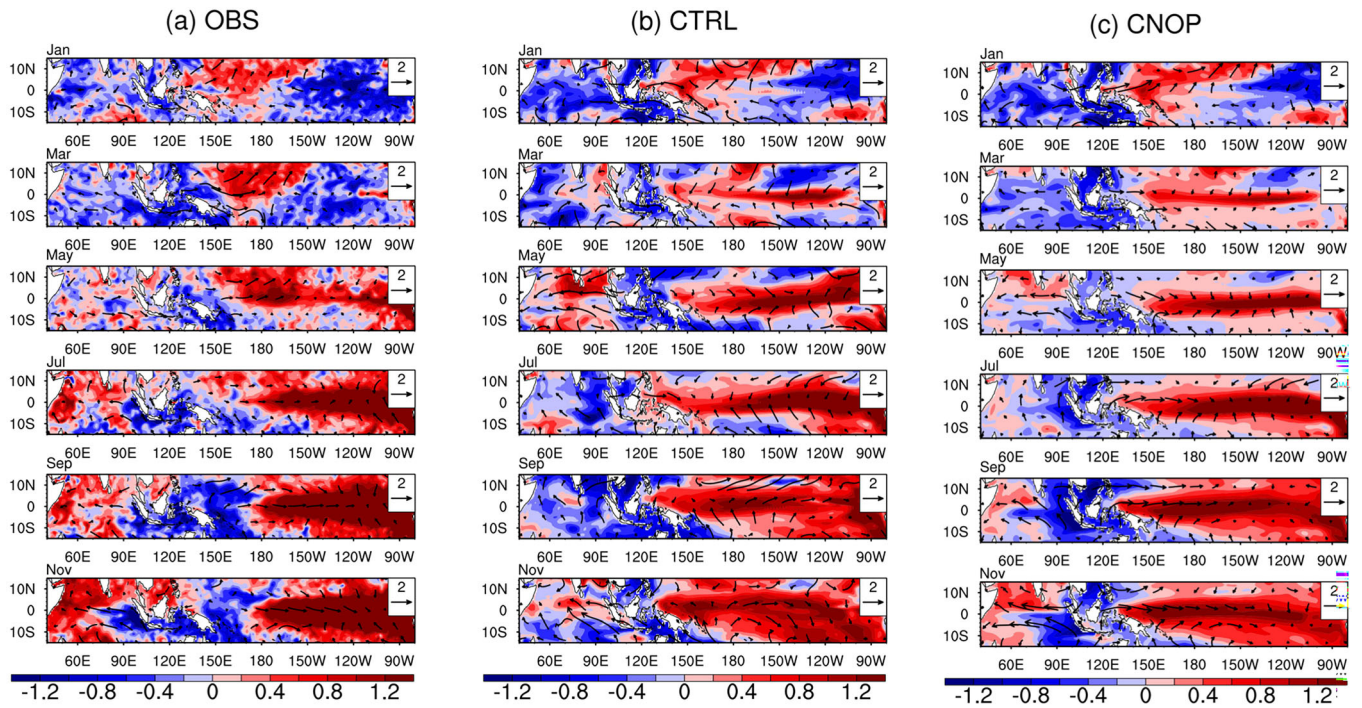
**FIGURE 7** Evolutions of SSTA (units:°C) and sea surface wind anomalies (units: m·s$^{-1}$) over the tropical Indian and Pacific oceans in 1997 in the (a) observation, (b) CTRL and (c) CNOP ensemble-mean forecast. [Colour figure can be viewed at wileyonlinelibrary.com]
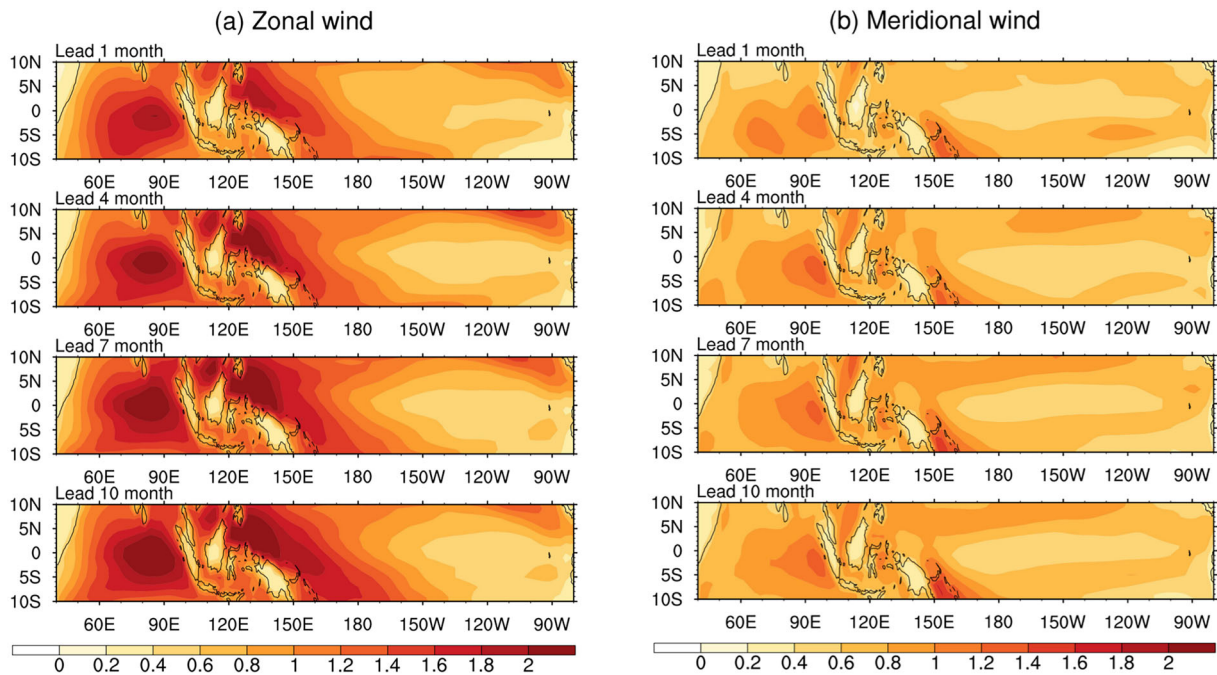


**FIGURE 8** Horizontal distributions of the wind spread (unit: m·s$^{-1}$) in the tropical Indian and Pacific oceans generated by the CNOP ensemble forecast for (a) zonal component and (b) meridional component at different lead months. The results are obtained for all of the predictions that were made during the period 1979–2008 regardless of their starting month. [Colour figure can be viewed at wileyonlinelibrary.com]

section, a comparison between the CNOP and CSV methods in IOD ensemble forecasting is conducted. The CSV initial perturbations, with the same magnitude as the CNOP initial perturbations, are applied to perturb global ocean temperatures at depths above 200 m. By adding and subtracting five CSV initial perturbations to
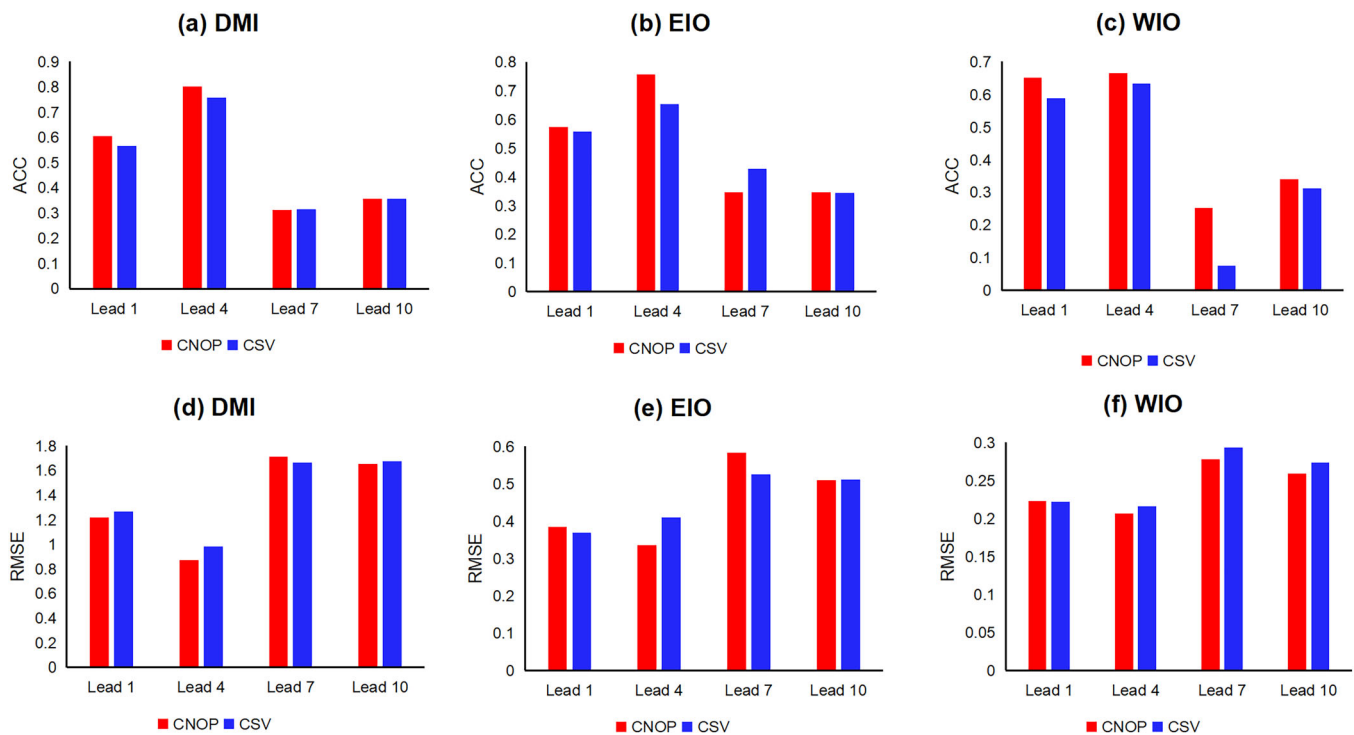
**FIGURE 9** The ACCs for the target season SON at different lead months in CNOP and CSV ensemble-mean forecasts for the (a) DMI, (b) EIO and (c) WIO; (d)–(f) corresponding RMSE values. [Colour figure can be viewed at wileyonlinelibrary.com]

and from the initial analysis field of the control forecast, the GFDL CM2p1 model is run for 12 months starting from four different months, together with the CTRL, resulting in a total of 11 ensemble members.

Given that IOD events typically peak during boreal autumn, the forecast skill for the target season SON (September–November) is examined in Figure 9. Predictions with lead times of 1, 4, 7 and 10 months were initiated in October, July, April and January, respectively. The analysis reveals that the ACC of the DMI for the CNOP ensemble-mean forecast is larger than that of the CSV method at lead times of 1 and 4 months, with the degree of improvement being 6.7% and 5.8%, respectively (Figure 10). The degree of improvement is calculated as the difference in forecast skill values between the CNOP and CSV experiments divided by the CSV forecast skill. That is, the CNOP ensemble-mean forecast displays higher skill compared to the CSV method for predictions starting from July and October. Conversely, the CNOP method for predictions starting from January and April presents a similar or slightly lower skill than the CSV method. From Figure 11, it is evident that the prediction errors in the CTRL exhibit large values at the initial time and maintain the large values before the SON in predictions initiated in July and October. These large errors motivate the strong nonlinear effects. And then, when the CNOP method, which fully considers the nonlinear

physical processes, is utilized in ensemble forecasts for these IOD predictions, the resulting ensemble forecasting members are able to better capture the nonlinear characteristics of error evolution compared to those made by the CSV method and achieve a higher ensemble forecast skill. In contrast, prediction errors are small before SON in the CTRL forecast initiated in April, and the nonlinear effects are weak; in this situation, the CSV method is sufficient to generate ensemble forecasting members that depict the weak nonlinear evolution of prediction errors, while the CNOP ensemble members, owing to their strong nonlinearity, may overestimate prediction errors and consequently yield a slightly lower forecast skill. Different from above start months, predictions errors initiated in January are small initially, which then significantly increase after July. Then, in the initial stage, the CNOP ensemble members tend to overestimate prediction error evolution, resulting in lower forecast skill. However, after July, they gradually demonstrate superior performance by considering nonlinear physical processes and increase the forecast skill, ultimately catching up with the forecast skill of the CSV method at the target season. Previous research has indicated that when initial perturbations are sufficiently small, the CNOP approach can be approximated by the SV method (Mu et al., 2003, 2006). This suggests that the aforementioned overestimation of prediction error evolution with the CNOP method
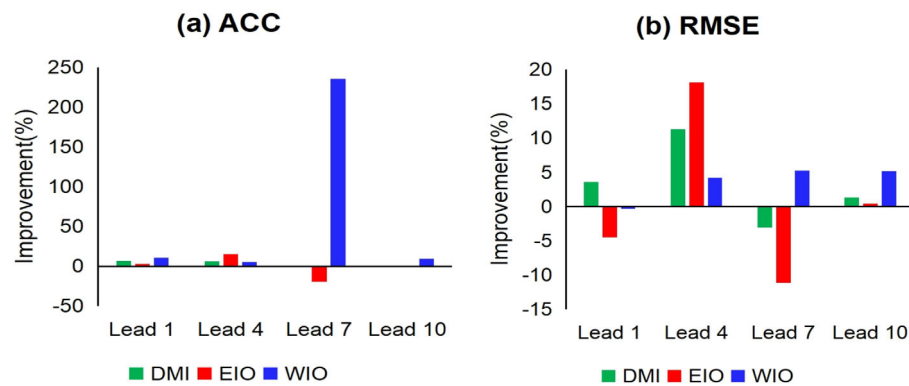
**FIGURE 10** (a) Degree of correlation skill improvement of CNOP ensemble-mean forecast to the CSV ensemble-mean forecast at different lead months for the DMI, EIO and WIO; (b) corresponding RMSE values. [Colour figure can be viewed at wileyonlinelibrary.com]
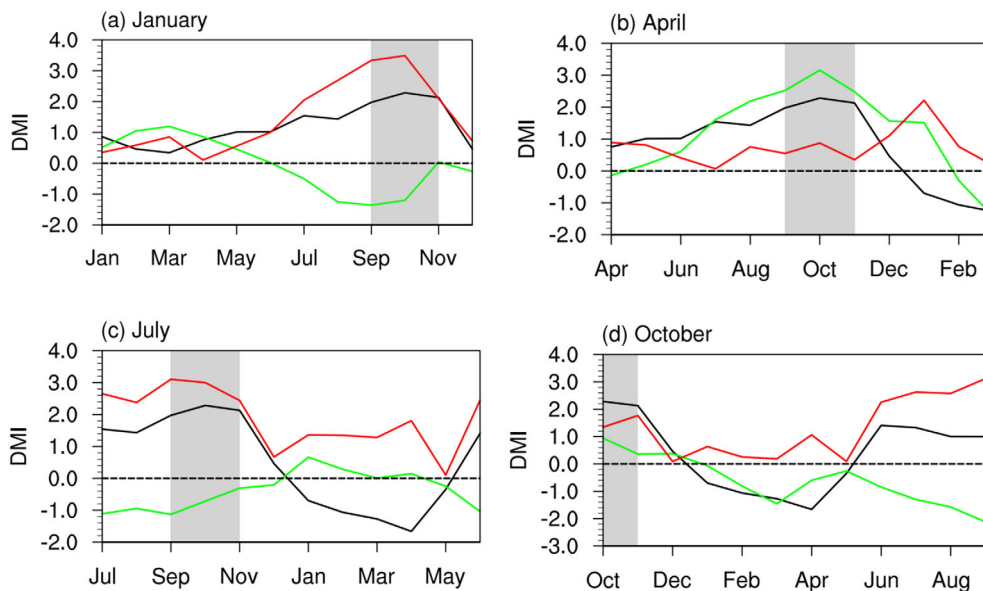


**FIGURE 11** Time variation of the DMI in observation (black) and the CTRL (green) for predictions starting from (a) January, (b) April, (c) July and (d) October; the red lines represent the prediction errors (i.e., the absolute values of the DMI difference between the CTRL and observation) in the CTRL; the grey bars signify the target season SON. [Colour figure can be viewed at wileyonlinelibrary.com]

may be attributed to the large constraint bounds exerted on initial perturbations. Consequently, if CNOP initial perturbations of appropriate magnitudes are adopted in predictions starting from January, they probably yield forecast skill comparable to the CSV method initially, with subsequent improvements after July leading to superior forecast skill. This hypothesis should be further investigation in future studies.

The analysis of the ACC in the EIO yields results that are consistent with those found in the DMI. The lower forecast skill in the CNOP method with a lead time of 7 months (i.e., initiated in April) can likely be attributed to the overestimation of error evolution due to the excessively large initial perturbations. Conversely, the ACC in the WIO in the CNOP ensemble-mean forecast is significantly larger than that in the CSV ensemble-mean forecast, showing significant improvements at all lead months, particularly notable at a 7-month lead time with the degree of improvement exceeding 200%. This suggests that the low correlation skill of IOD events in predictions starting from April is mainly due to the low forecast skill

in the EIO. Similarly, the RMSE in these experiments are also analysed and similar conclusions are drawn from the analysis.

Further analysis of the seasonal variability of forecast skill in both the CSV and CNOP ensemble forecasts is conducted (see Figure 5b,c). It is worth noting that the forecast skills in both the CNOP and CSV ensemble forecasts exhibit a significant seasonal dependence, emphasizing the presence of a WPB phenomenon. Specifically, the CNOP ensemble forecast skill decreases more rapidly throughout the boreal winter compared to the CSV ensemble forecast, suggesting a stronger WPB phenomenon. Additionally, the CNOP ensemble forecast has a higher correlation skill for predictions initiating in July and October, while showing a slightly lower or comparable forecast skill for those initiating in January and April, which is consistent with the results in Figure 9.

Although the CNOP-type initial perturbations are generated aimed at improving IOD ensemble forecast skill, they also lead to improved ACC skill in the tropical Pacific Ocean compared to the CTRL experiment as

FIGURE 12  ACC (a) and RMSE (b) of the Niño3.4 SSTAs for the CNOP and CSV ensemble forecast as functions of the lead time; ACC (c) and RMSE (d) improvement degree of CNOP ensemble forecast compared with the CSV method as functions of the lead time. The results are obtained for all of the predictions that were made during the period 1979–2008 regardless of their starting month. [Colour figure can be viewed at wileyonlinelibrary.com]
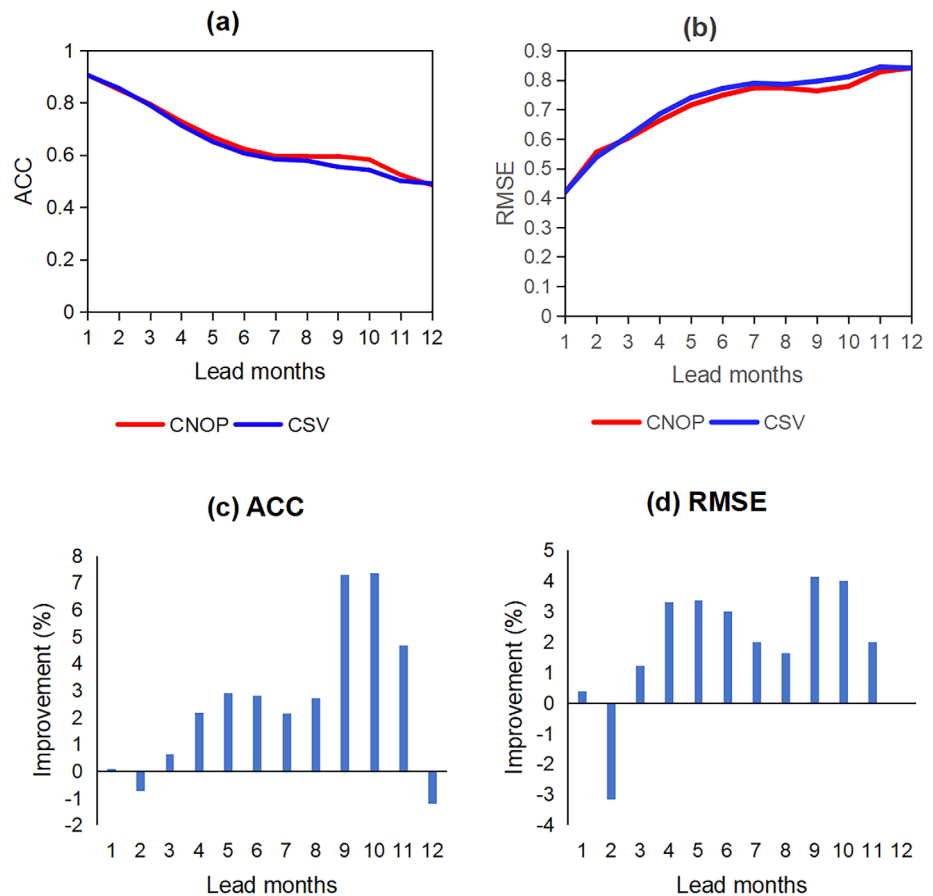
analysed in section 3. In this section, the ACC of Niño3.4 is further analysed to assess the ENSO forecast skill in different experiments (Figure 12). Specifically, the CNOP ensemble forecast outperforms the CSV ensemble forecast, particularly at long lead times, thus greatly prolonging the lead time of skilful forecast. Notably, the CNOP ensemble forecast exhibits the degree of improvement increasing to 7.4% over the CSV ensemble forecast. This further verifies its ability to capture the nonlinear evolution of ENSO and greatly improve forecast skill. As the close relation between the WIO and ENSO, the enhanced forecast skill of ENSO in the CNOP ensemble forecast, may contribute to the significant skill improvement in the WIO. Furthermore, the forecast skill improvement of the CNOP ensemble forecast for ENSO compared with the CSV method is significant at most lead months, with a 2.6% annual-mean improvement degree, which is larger than that for IOD. These findings from the ACC analysis are supported by similar conclusions drawn from the RMSE analysis.

## 4.2 | Reliability of the ensemble forecast

Previous studies have highlighted the importance of the ensemble spread being close to its RMSE for a reliable
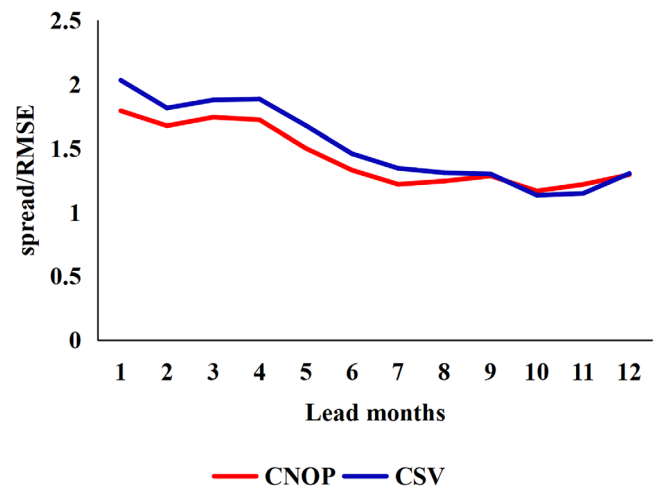
FIGURE 13  Evolution of the ratio (which is defined as spread/RMSE) values of the CNOP (red line) and CSV (blue line) ensemble forecast systems for the DMI as a function of the lead month. [Colour figure can be viewed at wileyonlinelibrary.com]

ensemble forecast system (Buizza et al., 2005). The ratio of the ensemble spread to RMSE serves as a measure of the reliability of the ensemble forecast system, with a ratio closer to 1 indicating higher reliability. Figure 13 illustrates the temporal variability of the ratio (spread/RMSE) for the DMI in both the CNOP and CSV ensemble
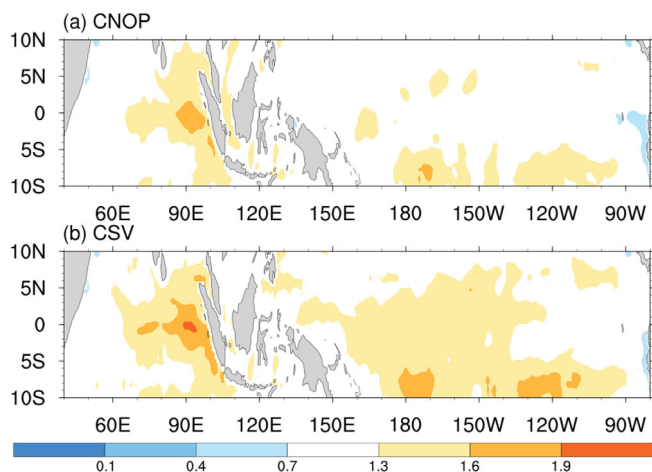
**FIGURE 14** The spatial distribution of the ratio (which is defined as spread/RMSE) for the DMI in the tropical Indian and Pacific oceans in the (a) CNOP, and (b) CSV ensemble forecast systems. The shaded area is above 1.3 or below 0.7, and the remaining areas represent values near 1. The results are obtained for all of the predictions that were made during the period 1979–2008 regardless of their starting month. [Colour figure can be viewed at wileyonlinelibrary.com]

forecasts. It is evident that the ratio is closer to 1 in the CNOP ensemble forecast at most lead months, confirming the higher reliability of the CNOP ensemble forecast system, which increases with increasing lead times. This indicates that the ensemble spread in the CNOP ensemble forecast system could better represent the prediction errors measured by the RMSE. Furthermore, the spatial distribution of the ratio in the tropical Indian and Pacific oceans is shown for both ensemble forecast systems in Figure 14. The ratios are close to 1 (i.e., 0.7 < ratio < 1.3) in the central-western Indian Ocean, as well as in the northern and equatorial Pacific Ocean in the CNOP ensemble forecast system, while these areas largely reduce in the CSV ensemble forecast system. This discrepancy implies that the CNOP ensemble forecast system has higher reliability and provides a more reliable estimate of prediction uncertainties. In contrast, the ratios exceed 1 in the eastern Indian Ocean and southern Pacific Ocean in both ensemble forecast systems, especially in the CSV ensemble forecast system, indicating presence of an underconfidence phenomenon. The cause of this underconfidence is not fully understood. Notably, despite the superior forecast skill exhibited by the CNOP method compared to the CSV method, the underconfidence phenomenon is still not overcome. Recent research by Duan et al. (2024) has demonstrated that the C-CNOP method can generate dynamically coordinated coupled initial perturbations, yielding more reliable ensemble members. This advancement could potentially narrow the gap between the ensemble spread and RMSE in ensemble forecasts. Consequently, further implementation of the C-CNOP method in the ensemble forecast may potentially overcome the underconfidence phenomenon and enhance the overall reliability of the forecast system.

# 5 | SUMMARY AND CONCLUSIONS

In the current study, by applying the CNOP method in generating initial perturbations and superimposing them on the initial field of the CTRL experiment, we conducted a 30-year ensemble forecast using the GFDL CM2p1 coupled model to examine the forecast skill of climate events.

First, the CNOP ensemble-mean forecast significantly improves the forecast skill of IOD events, particularly at longer lead times. Notably, a skilful forecast was achieved at a 4-month lead time, which is comparable with, or even better than, previous research findings. Furthermore, the advantage of the CNOP method is also reflected in the predictions for the WIO and EIO, with a skilful forecast at an 8- (5-) month lead time for the WIO (EIO). Additionally, we analysed the ACC for strong IOD events, revealing a skilful forecast at a 12-month lead time, outperforming many current state-of-the-art coupled models. The improvement of the CNOP method for strong IOD events becomes obvious at a long lead time, and this improvement is larger than that for all events. The findings regarding the RMSE were largely consistent with these conclusions.

The spatial patterns of ACC and RMSE are further examined, revealing that the CNOP ensemble-mean forecast significantly improves correlation skill and reduces prediction errors across the tropical Indian and Pacific oceans compared to the CTRL. This improvement becomes significant with the increasing lead time. Although the CNOP initial perturbations are generated aimed at improving IOD forecast skill, there is a notable enhancement in ENSO forecast skill as well. Moreover, the analysis of seasonal variation in forecast skill highlights a significant WPB in the CNOP ensemble forecast. Specifically, the CNOP ensemble-mean forecast shows a significantly greater improvement over the CTRL for predictions initiated in July and October.

Through an analysis of SSTAs and surface wind anomalies in different experiments, we delve into the mechanisms resulting in a higher forecast skill of the CNOP ensemble forecast. Our findings reveal that the CNOP ensemble forecast could better depict southeasterly wind anomalies in the EIO in March, which favours

the emergence of IOD event precursors. Additionally, the ensemble spread of zonal and meridional wind components in the CNOP ensemble forecast exhibits large values in the EIO, indicating its ability to capture the uncertainty of wind anomalies in this region, thereby providing more chances to capture IOD occurrences. Furthermore, in addition to surface wind anomalies, accurate predictions of heat flux fields are also crucial for improving the forecast skill of IOD events.

Second, the comparison of forecast skill between the CNOP and CSV ensemble forecasts is conducted with a focus on IOD and ENSO events. The findings reveal that the CNOP ensemble forecasts exhibit higher forecast skill for IOD predictions starting from July and October and show similar or slightly lower skill for predictions initiating in January and April. The CNOP method, which considers nonlinear physical processes, generates ensemble forecasting members that could better capture the nonlinear dynamic characteristics of error evolution for predictions starting from July and October with strong nonlinear effects, thereby achieving a higher forecast skill. Conversely, for predictions starting from April with weak nonlinear effects, the CSV-type initial perturbations are sufficient to generate ensemble forecasting members that depict the weak nonlinear evolution of prediction errors, while the ensemble members generated by the CNOP method tend to overestimate error evolution, resulting in a slightly lower forecast skill. Different from above start months, for predictions initiating in January, the CNOP ensemble members initially overestimate error evolution, leading to lower forecast skill in the early months; however, it gradually adjusts to capture the nonlinear error evolution after July, eventually catching up with the CSV ensemble forecast skill. Moreover, the ENSO forecast skill in the CNOP ensemble forecast is higher than that with the CSV method, particularly at longer lead times, with a more significant improvement compared to IOD events. Evaluation of the reliability of two ensemble forecast systems in terms of temporal and spatial variability indicates that the CNOP ensemble forecast system demonstrates higher reliability than the CSV ensemble forecast system, offering a more reliable estimate of prediction uncertainties. Notably, the ratios in the eastern Indian Ocean and southern Pacific Ocean are larger than 1, indicating the existence of an underconfidence phenomenon. By implementing the C-CNOP method and generating dynamically coordinated coupled initial perturbations, this underconfidence phenomenon might be overcome.

Based on above discussions, the CNOP method has significantly improved the forecast skill of climate events. It is important to note that, for convenience to compare with the CSV method, only the ocean temperature was perturbed to generate initial perturbations. The C-CNOP method, as proposed in Duan et al. (2024), could consider initial coupling effects among different components, capturing the initial coupling uncertainty information and greatly improving forecast skill, even when the coupling is at its weakest. Consequently, the potential application of the C-CNOP method incorporating additional components such as wind and salinity in IOD predictions, could lead to further improvement in IOD prediction skills. Additionally, to briefly validate the rationality of CNOP method in IOD ensemble forecasting and largely save the computer resources, a reduced number 5 IPs were utilized in the ensemble forecast. To determine the optimal sample size for achieving higher ensemble forecast skill and to assess whether the CNOP method maintains a significant advantage over other ensemble forecast methods under these conditions, further investigations are needed in the near future.

## AUTHOR CONTRIBUTIONS

**Rong Feng:** Investigation; formal analysis; writing – original draft; validation; writing – review and editing. **Wansuo Duan:** Methodology; formal analysis; writing – review and editing; supervision. **Lei Hu:** Investigation; formal analysis. **Ting Liu:** Formal analysis.

## ACKNOWLEDGEMENTS

## CONFLICT OF INTEREST STATEMENT

The authors declare no conflicts of interest.

## DATA AVAILABILITY STATEMENT

The data that support the findings of this study are available from the corresponding author upon reasonable request.

## ORCID

*Wansuo Duan* https://orcid.org/0000-0002-0122-2794

## REFERENCES

Anderson, J.L. (1997) The impact of dynamical constraints on the selection of initial conditions for ensemble predictions: low-order perfect model results. *Monthly Weather Review*, 125(11), 2969–2983.

Ansell, T., Reason, C.J.C. & Meyers, G. (2000) Variability in the tropical southeast Indian Ocean and links with southeast Australian winter rainfall. *Geophysical Research Letters*, 27(24), 3977–3980.

Buizza, R., Houtekamer, P.L., Pellerin, G., Toth, Z., Zhu, Y. & Wei, M. (2005) A comparison of the ECMWF, MSC, and NCEP global ensemble prediction systems. *Monthly Weather Review*, 133, 1076–1097. Available from: https://doi.org/10.1175/MWR2905.1

Cai, W., Yang, K., Wu, L., Huang, G., Santoso, A., Ng, B. et al. (2020) Opposite response of strong and moderate positive Indian Ocean Dipole to global warming. *Nature Climate Change*, 11, 27–32. Available from: https://doi.org/10.1038/s41558-020-00943-1

Carton, J.A. & Giese, B.S. (2008) A reanalysis of ocean climate using Simple Ocean Data Assimilation (SODA). *Monthly Weather Review*, 136(8), 2999–3017. Available from: https://doi.org/10.1175/2007MWR1978.1

Du, J., Zhou, B. & Levit, J. (2019) Measure of forecast challenge and predictability horizon diagram index for ensemble models. *Weather and Forecasting*, 34, 603–615.

Du, Y., Zhang, Y., Zhang, L., Tozuka, T., Ng, B. & Cai, W. (2020) Thermocline warming induced extreme Indian Ocean Dipole in 2019. *Geophysical Research Letters*, 47(18), e2020GL090079. Available from: https://doi.org/10.1029/2020GL090079

Duan, W.S., Hu, L. & Feng, R. (2024) Coupled conditional nonlinear optimal perturbations and their application to ENSO ensemble forecasts. *Science China Earth Sciences*, 67, 826–842. Available from: https://doi.org/10.1007/s11430-023-1273-1

Duan, W.S. & Huo, Z.H. (2016) An approach to generating mutually independent initial perturbations for ensemble forecasts: orthogonal conditional nonlinear optimal perturbations. *Journal of the Atmospheric Sciences*, 73(3), 997–1014.

Duan, W.S., Yang, L., Xu, Z. & Chen, J. (2023) Conditional nonlinear optimal perturbation: applications to ensemble forecasting of high-impact weather systems. In: Park, S.K. (Ed.) *Numerical weather prediction: East Asian perspectives*. Switzerland: Springer.

Evensen, G. (1994) Sequential data assimilation with a nonlinear quasigeostrophic model using Monte Carlo methods to forecast error statistics. *Journal of Geophysical Research*, 99(C5), 10143–10162. Available from: https://doi.org/10.1029/94JC00572

Feng, R., Duan, W.S. & Mu, M. (2014) The "winter predictability barrier" for IOD events and its error growth dynamics: results from a fully coupled GCM. *Journal of Geophysical Research: Oceans*, 119, 8688–8708. Available from: https://doi.org/10.1002/2014JC10473

Feng, R., Duan, W.S. & Mu, M. (2017) Estimating observing locations for advancing beyond the winter predictability barrier of Indian Ocean dipole event predictions. *Climate Dynamics*, 48, 1173–1185.

GFDL Global Atmospheric Model Development Team. (2004) The new GFDL global atmosphere and land model AM2-LM2: evaluation with prescribed SST simulations. *Journal of Climate*, 17, 4641–4673.

Griffies, S.M. (2009) *Elements of MOM4p1: GFDL Ocean Group*. Princeton, NJ: NOAA/Geophysical Fluid Dynamics Laboratory. Technical report: 6.

Houtekamer, P.L. & Derome, J. (1994) Prediction experiments with twomember ensembles. *Monthly Weather Review*, 122(9), 2179–2191.

Huang, P., Zheng, X.T. & Ying, J. (2019) Disentangling the changes in the Indian Ocean Dipole-related SST and rainfall variability under global warming in CMIP5 modes. *Journal of Climate*, 32(13), 3803–3818.

Hui, C. & Zheng, X.T. (2018) Uncertainty in Indian Ocean Dipole response to global warming: the role of internal variability. *Climate Dynamics*, 51, 3597–3611. Available from: https://doi.org/10.1007/s00382-018-4098-2

Huo, Z. & Duan, W. (2018) The application of the orthogonal conditional nonlinear optimal perturbations method to typhoon track ensemble forecasts. *Science China Earth Sciences*, 2, 376–388.

Kleeman, R., Tang, Y. & Moore, A. (2003) The calculation of climatically relevant singular vectors in the presence of weather noise. *Journal of the Atmospheric Sciences*, 60, 2856–2868.

Leutbecher, M. & Palmer, T.N. (2008) Ensemble forecasting. *Journal of Computational Physics*, 227(7), 3515–3539. Available from: https://doi.org/10.1016/j.jcp.2007.02.014

Liu, T., Song, X., Tang, Y., Shen, Z. & Tan, X. (2022) ENSO predictability over the past 137 years based on a CESM ensemble prediction system. *Journal of Climate*, 35, 763–777.

Lorenz, E.N. (1965) A study of the predictability of a 28-variable atmospheric model. *Tellus*, 17(3), 321–333.

Luo, J.J., Masson, S., Behera, S., Shingu, S. & Yamagata, T. (2005) Seasonal climate predictability in a coupled OAGCM using a different approach for ensemble forecasts. *Journal of Climate*, 18(21), 4474–4497.

Luo, J.J., Masson, S., Behera, S. & Yamagata, T. (2007) Experimental forecasts of the Indian Ocean Dipole using a coupled OAGCM. *Journal of Climate*, 20(10), 2178–2190. Available from: https://doi.org/10.1175/JCLI4132.1

Mu, M., Duan, W. & Wang, B. (2003) Conditional nonlinear optimal perturbation and its applications. *Nonlinear Processes in Geophysics*, 10, 493–501.

Mu, M., Duan, W., Xu, H. & Wang, B. (2006) Applications of conditional nonlinear opimal perturbation in predictability study and sensitivity analysis of weather and climate. *Advance in Atmospheric Sciences*, 23(6), 992–1002.

Saji, N.H., Goswami, B.N., Vinayachandran, P.N. & Yamagata, T. (1999) A dipole mode in the tropical Indian Ocean. *Nature*, 401(6751), 360–363.

Saji, N.H. & Yamagata, T. (2003) Interference of teleconnection patterns generated from the tropical Indian and Pacific Oceans. *Climate Research*, 25, 151–169.

Shi, L., Hendon, H.H., Alves, O., Luo, J.J., Balmaseda, M. & Anderson, D. (2012) How predictable is the Indian Ocean Dipole? *Monthly Weather Review*, 140(12), 3867–3884. Available from: https://doi.org/10.1175/MWR-D-12-00001.1

Song, Q., Vecchi, G.A. & Rosati, A.J. (2008) Predictability of Indian Ocean sea surface temperature anomalies in the GFDL coupled model. *Geophysical Research Letters*, 35(2), L02701. Available from: https://doi.org/10.1029/2007GL031966

Stockdale, T.N., Anderson, D., Balmaseda, M.A., Doblas-Reyes, F., Ferranti, L., Mogensen, K. et al. (2011) ECMWF seasonal forecast system 3 and its prediction of sea surface temperature. *Climate Dynamics*, 37(3–4), 455–471.

Toth, Z. & Kalnay, E. (1993) Ensemble forecasting at NMC: the generation of perturbations. *Bulletin of the American Meteorological Society*, 74(12), 2317–2330.

Wajsowicz, R.C. (2005) Potential predictability of tropical Indian Ocean SST anomalies. *Geophysical Research Letters*, 32(24), L24702. Available from: https://doi.org/10.1029/2005GL024169

Webster, P.J., Moore, A.M., Loschnigg, J.P. & Leben, R.R. (1999) Coupled ocean–atmosphere dynamics in the Indian Ocean during 1997–98. *Nature*, 401(6751), 356–360.

Zhang, H., Duan, W.S. & Zhang, Y. (2023) Using the orthogonal conditional nonlinear optimal perturbations approach to address the uncertainties of tropical cyclone track forecasts generated by the WRF model. *Weather and Forecasting*, 38, 1907–1933.

Zhao, M. & Hendon, H.H. (2009) Representation and prediction of the Indian Ocean dipole in the POAMA seasonal forecast model. *Quarterly Journal of the Royal Meteorological Society*, 135(639), 337–352. Available from: https://doi.org/10.1002/qj.370

Zhu, J., Huang, B., Balmaseda, M.A., Kinter, J.L., III, Peng, P., Hu, Z.Z. et al. (2013) Improved reliability of ENSO hindcasts with nulti-ocean analyses ensemble initialization. *Climate Dynamics*, 41, 2785–2795.

Zhu, J., Huang, B., Kumar, A. & Kinter, J.L. (2015) Seasonality in prediction skill and predictable pattern of tropical Indian Ocean SST. *Journal of Climate*, 28(20), 7962–7984. Available from: https://doi.org/10.1175/JCLI-D-15-0067.1